

# Use of Non-Matrix Matched Reference Materials for the Accurate Analysis of Calcium Carbonate by LA-ICP-MS

Jennifer A. Thompson (1, 2)\* , Jay M. Thompson (2, 4) , Karsten Goemann (3), Elena Lounejeva (2), David R. Cooke (1, 2) and Leonid Danyushevsky (1, 2)

(1) Transforming the Mining Value Chain, an ARC Industrial Transformation Hub, University of Tasmania, Private Bag 79, Hobart, Tasmania, Australia

(2) CODES, Centre for Ore Deposit and Earth Sciences, University of Tasmania, Private Bag 79, Hobart, Tasmania, Australia

(3) Central Science Laboratory, University of Tasmania, Private Bag 74, Hobart, Tasmania, 7001, Australia

(4) Present address: Geology, Geophysics and Geochemistry Science Center, US Geological Survey, Denver Federal Center, Denver, CO, 80225, USA

\* Corresponding author. e-mail: j.a.thompson@utas.edu.au

Advances in laser ablation inductively coupled plasma-mass spectrometry have improved analytical precision for mineral analysis, expanding geological interpretations from LA-ICP-MS results. However, with improvements in analytical precision, systematic errors from calibration can become more obvious and affect data quality. To improve the accuracy of the LA-ICP-MS technique, a fully quantified method is presented for the analysis of minerals with a CaCO<sub>3</sub> matrix. An in-house calcite sample (P-Cal) was developed with an independently constrained composition and compared with measurement results from LA-ICP-MS analysis, generated using multiple spot sizes, laser fluences and calibration methods. For many elements, calibration against NIST SRM 612 as a calibration reference material and USGS GSD-1G and USGS BCR-2G as secondary reference materials (calibration B) provided the best accuracy for CaCO<sub>3</sub> analysis. Ablation rates and element yield (ICP-MS signal intensity in counts per second for a given isotope relative to the mass fraction of the respective element) in calcium carbonate closely resembles NIST SRM 612; however, the down-hole fractionation curves of USGS BCR-2G (basaltic glass matrix) are a better fit for carbonate. Variations in accuracy for measurements at different spot sizes are negligible compared with the other effects discussed. Additionally, ablation characteristics for powdered crystals versus large fragments produce a negligible effect on the accuracy of the results for calcium carbonate.

Keywords: calcium carbonate, LA-ICP-MS, chemical analysis, method validation, mineral chemistry.

Received 26 Jan 21 – Accepted 10 Sep 21

Calcium carbonate (CaCO<sub>3</sub>) can be present in various mineralogical forms, called trimorphs (e.g., calcite, aragonite and vaterite) depending on the conditions at which the crystal grew. The chemistry of these calcium carbonate minerals can provide insight into, for example, marine environments (e.g., Mitsuguchi *et al.* 1996, Druffel 1997, Wyndham *et al.* 2004, Frimmel 2009), palaeoclimate conditions (e.g., Griffiths *et al.* 2010, Tremaine and Froelich 2013, Barnet *et al.* 2020) and ore deposit formation (e.g., Kontak and Jackson 1995, Vaughan *et al.* 2016, Kalliomaki *et al.* 2019). Fine-scale variations of carbonate chemistry require the use of microanalytical tools such as laser ablation inductively coupled plasma-mass spectrometry (LA-ICP-MS),

an analytical technique for *in situ* determination of elemental and isotopic compositions of solid materials. The LA-ICP-MS technique is used widely for mineral trace element measurement (Izbekov *et al.* 2002, Browne *et al.* 2006, Barker and Cox 2011, He *et al.* 2019) due to its relatively low detection limits compared with other *in situ* techniques.

Development of an accurate method for mineral chemical analysis requires a comprehensive understanding of the potential sources of uncertainty within a LA-ICP-MS analytical method, and includes parameters such as laser fluence, laser spot size, calibration materials and ICP-MS sampling conditions (Norris and Danyushevsky 2018). Analysis by LA-

ICP-MS aiming to determine the elemental composition of minerals is commonly calibrated using reference glasses (e.g. NIST SRM 612, Jochum *et al.* 2011) as these are virtually homogenous in composition. However, use of glass reference materials often leads to a mis-match of the major element composition or 'matrix' between calibration materials and mineral targets. Because LA-ICP-MS is subject to issues of non-representative sampling at the ablation site (Jackson *et al.* 2004, Kuhn *et al.* 2010, Košler *et al.* 2014) and during aerosol digestion in the ICP (Guillong and Günther 2002, Fietzke and Frische 2016), there can occur inaccuracies due to matrix difference between calibration materials and unknowns. Different materials will also interact differently with the laser beam (Russo *et al.* 2000) to produce variable yields, defined here as the signal intensity of a specific isotope per unit mass fraction of the respective element (corrected for isotopic abundance) in the material. Some elements behave differently to others during laser ablation analysis, producing elemental fractionation, which will vary depending on the matrix analysed (Fryer *et al.* 1993, Jackson 1996, Guillong and Günther 2002, Kros拉克ova and Günther 2006, Gaboardi and Humayun 2009, Kuhn *et al.* 2010). Matrix-matched calibration materials would be ideal for accurate analysis, however, homogenous minerals that also contain adequate mass fractions of all the elements of interest are difficult to locate in the natural environment.

Previous investigations have shown the suitability of glass reference materials to calibrate carbonate compositions at large laser spot sizes  $\sim 100\ \mu\text{m}$  and greater (Hathorne *et al.* 2008, Mertz-Kraus *et al.* 2009, Strnad *et al.* 2009). Chen *et al.* (2011) demonstrated that glass reference materials are suitable with accuracies within 5–10% of published values for calcium carbonate analysis; however, a systematic bias of 10–20% was observed at  $32\ \mu\text{m}$ . Jochum *et al.* (2012) showed that glass reference material is generally suitable for calcite, but some elements require a carbonate reference material due to spot size effects and element fractionation (e.g., Pb). We investigate the suitability of using glass reference materials to calibrate carbonate compositions at smaller spot sizes (20 and  $30\ \mu\text{m}$ ) by using a large calcite megacryst (P-Cal, for 'pink calcite') with mass fractions of twenty-six elements above the detection limit of the method applied in this study. The P-Cal sample is from the Tribulation quarry in Queensland, NSW Australia,  $\sim 11\ \text{km}$  north of the Mary Kathleen uranium mine in the Mary Kathleen Fold Belt (Page 1983). The sample was collected by Professor David Cooke and is from a high temperature pod of calcite hosted in the Corella Formation (Oliver *et al.* 1993). We analysed chips (mm in size) and pressed pellets of powdered P-Cal calcite. The purpose of this study is to provide a detailed method for quantification of

carbonate by LA-ICP-MS including optimal laser conditions and reference materials. We also discuss the effects of ablating millimetre sized crystal chips versus powdered material for quantitative analysis of calcite as well as aragonite to assess if there are any differences in ablation characteristics between these two forms of calcium carbonate.

## Experimental methods

---

The elemental composition of P-Cal was defined by solution ICP-MS, XRF and electron probe microanalysis (EPMA). The defined P-Cal values were then compared with laser ablation ICP-MS results to determine the best practices for determination of accurate calcium carbonate chemistry results at large and small spot sizes. Additionally, several calcium carbonate samples were evaluated, including a marble with major element compositions verified by EPMA, an aragonitic otolith and the pressed pellet calcium carbonate reference material USGS MACS-3.

### Sample preparation

A large megacryst of calcite (P-Cal) was broken into multiple size fractions via an agate mortar and pestle. Chips that were  $\sim 1\text{--}5\ \text{mm}$  in diameter and appearing inclusion free under binocular microscope, were hand-picked for further use. The chips were randomly divided into aliquots for solution ICP-MS, XRF, and chips mounted in epoxy for microprobe and LA-ICP-MS analysis. Samples mounted in epoxy were polished with 600–2000 grit Si-C sandpaper, cleaned in de-ionised water with a sonicator, and then polished using  $1\ \mu\text{m}$  diamond paste. The sample mount was cleaned and sonicated several times in high purity methanol followed by several rinses and sonicating using de-ionised water. The sample mount was then dried at  $100\ ^\circ\text{C}$  for 1 h and stored under vacuum in a desiccator. A sample of Bluefin tuna otolith (adult specimen) and a marble sample from the marble halo to the Grasberg Intrusive Complex, Indonesia (Leys *et al.* 2012) were mounted in epoxy and prepared in a similar fashion to the P-Cal chips.

### XRF bulk analysis

A representative 20 g aliquot of P-Cal chips were picked and powdered by hand in an agate mortar and pestle using ultra high purity methanol as a grinding aide. The powder was ground to fineness so that no grit was felt by fingers on a small test aliquot. From this representative 20 g powder, an aliquot of  $\sim 10\ \text{g}$  was mixed with  $\sim 10\%$  PVA (poly vinyl alcohol) binder to ensure robust pill formation and pressed in the Spex X-Press 3650 hydraulic press at 10 tons using a 30 mm diameter die for 3 min and pressure

released slowly over 2 min. A second aliquot of ~ 2 g of the representative powder was pressed at 6 tons in a 15 mm die, but no binder added. In both pressed pellets a 6 µm thick Mylar film was used to cover the faces of the pressed pellet to avoid any metal contamination from the steel press on to the sample surface. The 30 mm pressed pellet was utilised for trace element analysis by XRF, while the 15 mm diameter pressed pellet was mounted in epoxy for LA-ICP-MS analysis without any epoxy covering the surface of the pressed pellet. Thus, there was no need to polish the sample and risk contamination of the surface. A pressed pellet of the USGS MACS-3 calcium carbonate reference material was also mounted in epoxy in a similar fashion to the P-Cal pressed pellet, also without the use of polishing.

Trace and major element compositions were obtained from a pressed powder pellet and glass disc respectively using an Axios Advanced wavelength dispersive XRF housed at the University of Tasmania. Major element compositions of the P-Cal calcite megacryst were determined via fused Li-B glass disc using powder prepared for XRF pressed pellets. The Li-B glass disc was prepared by mixing 0.44 g pf powder with 3.96 g high purity dilithium tetraborate and 0.606 g of LiNO<sub>3</sub> (pipetted as a 1 ml saturated LiNO<sub>3</sub> solution). The mixture is fused in a Claisse M4 fusion instrument for 12 min with an optimised temperature (1000 °C) and mixing procedure to ensure homogeneity of glass discs and to prevent loss of volatile elements during fusion.

Calibrations for major and trace element measurements were done using a combination of more than thirty international reference materials, synthetically prepared discs from single element oxide powders, and standard addition of Ca, Ba, Sr, Cu, Pb, Zn, As, Cr, V, Ni and Co to in-house reference materials TASBAS, TASDIOR and international reference materials JLS-1 and JDo-1. Elements measured in the major element routine were Si, Ti, Al, Fe, Mn, Mg, Ca, Na, K, P, S, Ba, Sr, Cu, Pb, Zn, As, Cr, V, Ni, Co and F. Those included in the trace element routine were Sc, Ti, V, Cr, Ni, Co, Cu, Zn, Ga, Ge, As, Se, Br, Rb, Sr, Y, Nb, Zr, Mo, Ag, Cd, Sn, Sb, Te, Ba, La, Ce, Nd, W, Tl, Pb, Bi, Th and U. Where there is overlap in elements between the two routines, elements are reported using the trace element routine unless the mass fraction is above 2000 µg g<sup>-1</sup>. Results for major element analysis were obtained using a carbonate-specific XRF calibration. Limestone and dolomite reference materials JLS-1 and JDo-1 were analysed as both glass discs (major elements) and pressed pellets (trace elements) for quality control. Elements in P-Cal that were below the detection limit of XRF included F, Na, Al, P, K, Sc, V, Cr, Co, Ga, Ge, As, Se, Mo, Ag, Cd, Sn, Sb, Te, Bi and U (Appendix S1).

## Solution ICP-MS bulk analysis

Solution ICP-MS data were obtained for seven different chips of calcite and four digestions of powder (Appendix S2). All work was performed in the Class 100 clean room at CODES Analytical Laboratories, University of Tasmania. Sample aliquots of 100 mg were placed into pre-cleaned 7 ml PTFE beakers with 1 ml of ultrapure water (18.2 MΩ cm, Milli-Q water) and 2 ml of Seastar grade 16 mol l<sup>-1</sup> HNO<sub>3</sub>, and heated at 120 °C for 12 h. Samples were cooled and sonicated to ensure dissolution, then gravimetrically diluted by 1500× into a final solution of 2% HNO<sub>3</sub>. Samples were spiked with 10 ng ml<sup>-1</sup> of Ge, In, Rh and Re as internal standard elements to correct for any instrument drift and sample dependent matrix loading effects in the ICP.

A high purity, single element solution (HPS Spex, CertiPrep) of Ca was added to TASBAS (Tasmanian basalt; Falloon *et al.* 2007, Leslie *et al.* 2009) and to a prepared calibration solution containing 2.5 ng ml<sup>-1</sup> of the measured elements. In addition to P-Cal, a set of international reference materials were dissolved and analysed as unknowns for quality control purposes: Cal-S (calcite), OPC-1 (Ordinary Portland Cement, GeoPT26), JLS-1 (limestone) and JDo-1 (dolomite). Analysis was performed on an Agilent 7700 quadrupole ICP-MS using a collision cell with helium gas addition at 2.4 ml min<sup>-1</sup> to minimise polyatomic interferences (e.g., <sup>40</sup>Ca<sup>16</sup>O<sup>1</sup>H on <sup>57</sup>Fe). Instrument calibration was performed using multi-element solutions (Spex CertiPrep, Metuchen, NJ, USA) gravimetrically prepared at 0.5, 1, 5, 10 and 20 ng ml<sup>-1</sup> concentration. Raw data in counts per second (cps) were corrected for oxide production from Ba, Ce, Pr, Nd, Gd, Tb and Er. Instrument drift correction was performed on a multi-elemental solution of 10 ng ml<sup>-1</sup> of each measured element. Procedural blanks were monitored for several elements and found negligible in most cases: REE blanks of 0.001–0.004 ng g<sup>-1</sup>, Fe blanks of ~ 0.01 ng g<sup>-1</sup>, Ca and Mg blanks between 0.7 and 0.9 ng g<sup>-1</sup> compared with > 3 orders of magnitude higher signal in the P-Cal sample. Procedural blanks were subtracted during data reduction. Elemental compositions of the analysed reference materials treated as unknowns agreed within the range of published values (GeoReM, Jochum *et al.* 2005).

## Electron probe microanalysis and SEM bright phase search

The mounts of chips of the P-Cal megacryst and a marble sample embedded in epoxy resin were carbon coated with ~ 20 nm thick coat and determined by Electron

Microprobe Analysis (EPMA) at the Central Science Laboratory (CSL), University of Tasmania (Appendix S1). A JEOL JXA-8530F Electron Microprobe with a field emission source and five wavelength dispersive spectrometers were used for the analysis with a defocused electron beam (~ 30  $\mu\text{m}$  spot size) using an accelerating voltage of 15 kV and beam current of 30 nA. No change in X-ray intensities due to damage by the electron beam was observed at these conditions for the duration of the analysis (30 s). Elements determined by EPMA were Mg ( $K_{\alpha}$ , using TAPL crystal), Ca ( $K_{\alpha}$ , using PETJ crystal), Mn ( $K_{\alpha}$ , using LiFL crystal) and Fe ( $K_{\alpha}$ , using LiFL crystal). For the calibration of different elements, the following reference materials were utilised: Broken Hill Rhodonite ( $\text{MnSiO}_3$ , P&H Developments) for Mn, Minas Gerais Hematite (Harvard 92649) for Fe, San Carlos Olivine (NMNH 111312-44) for Mg and Calcite (NMNH 136321) for Ca. Each element had a 30 s peak and off-peak counting time with a linear off-peak correction method for Ca and Fe and an exponential method for Mg and Mn. Oxygen was calculated by stoichiometry with elemental C calculated as 0.3333 atoms relative to 1.0 atom of O. Individual results are normalised to 100% analytical total. Secondary carbonate reference materials run with P-Cal include Dolomite (Harvard 105064, McGuire *et al.* 1992), Siderite (NMNH R2460, Jarosewich and Macintyre 1983), and an internal-lab reference material Rhodochrosite Santa Eulalia (Cannon Microprobe, Seattle, WA, USA).

A bright phase search was performed using backscatter electron (BSE) images on an FEI Quanta 450 with a field emission source and using an Oxford EDS detector at the USGS Denver Microbeam Laboratory (DML) in Denver, Colorado. A 15 kV accelerating voltage and a working distance of 11 mm were used. The bright phase search parameters were such that any bright phase relative to calcite with dimensions of 0.42  $\mu\text{m}$   $\times$  0.42  $\mu\text{m}$  in BSE would be detected and measured by EDS to identify phase. Bright phase searches were performed on a representative eleven calcite grains (or portions of grains). Due to the relatively small inclusion size (typically < 1  $\mu\text{m}$ ) to the beam size (5  $\mu\text{m}$ ), there was overlap with the calcite host; however, this did not affect the qualitative identification of phases. A quantitative estimate of surface area for each inclusion type was derived from the BSE images and area of the calcite grains in the search was measured using the software Image J (Norris and Danyushevsky 2018).

### LA-ICP-MS analysis

Four calcium carbonate materials (P-Cal, Marble, Otolith and USGS MACS-3) were analysed along with glass reference materials (NIST SRM 612, USGS BCR-2G, USGS

GSD-1G) by LA-ICP-MS at CODES Analytical Laboratories, University of Tasmania. For the reference materials the preferred values of the GeoReM database (application version 27, January 2020, Jochum *et al.* 2011) were applied. The laser ablation system was an ASI (now Applied Spectra, Fremont, CA, USA) Resolution SE 155 with an ATL-EX ArF excimer laser source operating at 193 nm wavelength and a 5–8 ns pulse width. The laser ablation system was equipped with a large format, two-volume ablation cell that houses up to twenty 25-mm sample rounds. The ablation takes place in a helium atmosphere (flow rate 350 ml  $\text{min}^{-1}$ ) within the fixed second volume funnel (~ 9  $\text{cm}^3$ ). The helium aerosol derived from the ablation was immediately mixed with argon (1.05 l  $\text{min}^{-1}$ ) in the funnel, wherein the gas-particle mixture exited the ablation cell and was sent to the 'squid' (Muller *et al.* 2009) to smooth out individual laser pulses. The aerosol and gases then enter an Agilent 7900 quadrupole ICP-MS. The Agilent 7900 was tuned daily for maximum sensitivity using a line scan on the NIST SRM 612 glass (40  $\mu\text{m}$ , 3  $\mu\text{m}$   $\text{s}^{-1}$  and ~ 3.5  $\text{J cm}^{-2}$  laser fluence) while achieving  $\text{U}^+/\text{Th}^+ \sim 1$ ,  $\text{ThO}^+/\text{Th}^+ \sim 0.18\%$ ,  $^{44}\text{Ca}^{2+}/^{44}\text{Ca}^+ \sim 0.2\%$ , a 43/57 mass ratio > 100 (Thompson *et al.* 2020) and peak widths of ~ 0.7 amu at 10% height. Typical ablation yield at these tune conditions was ~ 9400 cps per  $\mu\text{g g}^{-1}$  for  $^{238}\text{U}$ .

To assess calibration methods and best analytical conditions to analyse calcium carbonate by LA-ICP-MS, two different tests were conducted. The purpose of test #1 was to assess the best calibration strategy for carbonate. In test #1 P-Cal chips and pressed pellet were analysed as unknowns measured at a 20, 30 and 60  $\mu\text{m}$  diameter spot size, 5 Hz repetition rate and 3.5  $\text{J cm}^{-2}$  laser fluence that was measured by an external metre above the laser cell window prior to analysis with a 9% loss measured through the window that is factored in to the calculated fluence. Isotopes measured were:  $^{24}\text{Mg}$ ,  $^{29}\text{Si}$ ,  $^{39}\text{K}$ ,  $^{42}\text{Ca}$ ,  $^{43}\text{Ca}$ ,  $^{47}\text{Ti}$ ,  $^{55}\text{Mn}$ ,  $^{57}\text{Fe}$ ,  $^{59}\text{Co}$ ,  $^{60}\text{Ni}$ ,  $^{63}\text{Cu}$ ,  $^{66}\text{Zn}$ ,  $^{85}\text{Rb}$ ,  $^{88}\text{Sr}$ ,  $^{89}\text{Y}$ ,  $^{137}\text{Ba}$ ,  $^{139}\text{La}$ ,  $^{140}\text{Ce}$ ,  $^{146}\text{Nd}$ ,  $^{147}\text{Sm}$ ,  $^{153}\text{Eu}$ ,  $^{157}\text{Gd}$ ,  $^{163}\text{Dy}$ ,  $^{166}\text{Er}$ ,  $^{172}\text{Yb}$ ,  $^{175}\text{Lu}$ ,  $^{208}\text{Pb}$ ,  $^{232}\text{Th}$ ,  $^{238}\text{U}$  with dwell times between 10 and 20 ms and a total quadrupole sweep time of 0.496 s.

All data reductions were performed using LADR (Norris and Danyushevsky 2018) (<https://norsci.com/?p=ladr>) with Ca as the internal standard element, and all cations normalised to 100% oxide total assuming stoichiometric proportions of carbon in calcite with negligible contents of organic carbon. A correction was applied to  $^{57}\text{Fe}$  due to the production of  $^{40}\text{Ca}^{16}\text{O}^1\text{H}^+$  (Thompson *et al.* 2020) using a fish otolith composed of aragonite with Fe contents < 1  $\mu\text{g g}^{-1}$  that was previously confirmed via LA-ICP-TOF-MS with peak resolution  $r = \sim 2500$  ( $r = m/\Delta m$ , where  $m$  is

the centre and  $\Delta m$  the full width of the mass peak at half maximum). The removal of the interference on  $^{57}\text{Fe}$  was performed in LADR on all reference materials and unknowns. Other CaO interferences on Co and Ni were found to be below limit of detection in this same fish otolith. Each analysis consisted of five shots of pre-ablation to clean the sample surface, 20 s of washout, the ICP-MS receives a trigger to collect data for a 30 s gas blank followed by a 60 s ablation. A total of about twenty-five 1 mm-sized chips of the P-Cal megacryst were analysed for test #1 that included four laser spots per chip per spot size for a total of 300 measurements on P-Cal. The NIST SRM 612 reference glass was analysed at each spot size ( $n = 22$ ) and the 60  $\mu\text{m}$  spot size was analysed throughout test #1 to correct for instrument drift ( $n = 22$ ). USGS reference glasses USGS BCR-2G and USGS GSD-1G were analysed at each spot size as well ( $n = 22$ ), while the USGS MACS-3 pressed pellet was analysed at the 30  $\mu\text{m}$  spot size only ( $n = 15$ ). Reference materials were run in blocks between thirty to fifty unknowns (P-Cal chips) or every  $\sim 40$ –60 min and measurements at different spot sizes were arranged with increasing size during the run to minimise any sample carry-over.

A primary calibration was used to correct for instrument drift and obtain instrument element relativity factors to convert data from cps to  $\mu\text{g g}^{-1}$  based upon the equations of Longerich *et al.* (1996). The secondary calibration is used to account for matrix and spot size effects. The secondary calibration was created using the ratio of the accepted to the measured values of the secondary reference materials for each isotope measured and multiplying by the unknowns. Where secondary RM correction is done using multiple reference materials (e.g., USGS BCR-2G and USGS GSD-1G) a mean correction factor is calculated and applied to the unknowns. The primary and secondary calibrations were both done in LADR.

For test #1 there were four different calibration methods employed on the exact same set of 300 measurements to isolate the effect of calibration (Table 1). A: a primary calibration on the NIST SRM 612 glass matching each spot size; for example, 20  $\mu\text{m}$  P-Cal spots were calibrated using 20  $\mu\text{m}$  NIST SRM 612 spots, and no secondary RM correction was applied. B: a primary calibration using the NIST SRM 612 glass at a 60  $\mu\text{m}$  spot size and a secondary correction for differences in spot size for the unknowns using the mean correction factors of USGS BCR-2G and USGS GSD-1G for each spot size (20, 30 and 60  $\mu\text{m}$ ). C: a primary calibration using the NIST SRM 612 glass at a 60  $\mu\text{m}$  spot size and a secondary correction for the difference in spot size for the unknowns

using the NIST SRM 612 measured at each respective spot size (except 60  $\mu\text{m}$  as this is already spot size-matched). D: similar to B and C, but using the USGS MACS-3 preferred values to apply a secondary correction for spot size and only for the measurements done at 30  $\mu\text{m}$ .

The purpose of test #2 was to assess the yield and ablation rate for a variety of carbonate materials relative to glass reference materials for a range of laser fluences: 1.5, 2.5, 3.5, 4.5 and 5.5  $\text{J cm}^{-2}$ ; at three different laser spot sizes: 20, 30 and 60  $\mu\text{m}$  diameters, and all measurements were conducted at 5 Hz laser repetition rate, which generated fifty total shots per ablation. The materials analysed included reference glasses NIST SRM 612, USGS GSD-1G and USGS BCR-2G; while carbonate materials included P-Cal calcite chips and pressed pellet, GIC Marble, Otolith and USGS MACS-3. Each sample was analysed in duplicate for each energy, at each spot size. No pre-ablation was performed, with a 10 s gas blank followed by a 10 s ablation. The isotopes measured for test #2 were  $^{24}\text{Mg}$ ,  $^{29}\text{Si}$ ,  $^{43}\text{Ca}$ ,  $^{55}\text{Mn}$ ,  $^{57}\text{Fe}$ ,  $^{88}\text{Sr}$ ,  $^{137}\text{Ba}$ ,  $^{140}\text{Ce}$ ,  $^{172}\text{Yb}$ ,  $^{208}\text{Pb}$ ,  $^{232}\text{Th}$  and  $^{238}\text{U}$  with dwell times between 10 and 20 ms and a quadrupole sweep time of 0.162 s. Because the main purpose of test #2 was not quantification of results, but to assess variances in yield and ablation rate at the different laser conditions (spot size and fluence), the element list was kept short to only include elements that might be useful in estimating yield based upon their high abundance in carbonate, and the ablation was kept short to aide in laser crater depth measurements. Laser crater depths were measured using a Bruker Contour GT-K light interferometer with a 50 $\times$  objective and a 0.55 $\times$  magnifier.

**Table 1.**  
Summary of four calibration methods discussed in the text

Method	Primary calibration		Secondary calibration	
	Material	Spot size	Material	Spot size
A	NIST SRM 612	Matching unknowns	None	
B	NIST SRM 612	60 $\mu\text{m}$	USGS GSD-2G and BCR-2G	Matching unknowns
C	NIST SRM 612	60 $\mu\text{m}$	NIST SRM 612	Matching unknowns
D	NIST SRM 612	60 $\mu\text{m}$	USGS MACS-3	30 $\mu\text{m}$

Calibration material matching spot size implies the calibration material was run at the same spot size as unknowns in duplicate and bracketing unknowns. In test 1, most reference materials were analysed at 5 Hz, 3.5  $\text{J cm}^{-2}$  and at spot sizes of 20, 30 and 60  $\mu\text{m}$ . USGS MACS-3 was only analysed at 30  $\mu\text{m}$ .

## Results and discussion

### Assignment of P-Cal working values

In order to assess the optimum laser conditions for carbonate analysis, the level of homogeneity and chemical composition was established for an in-house sample (P-Cal). To ensure accurate characterisation of the P-Cal calcite, multiple elements were assessed by multiple analytical techniques. Calcium, Mg, Fe and Mn mass fraction in P-Cal were determined by solution ICP-MS, electron microprobe and XRF analyses. The resulting P-Cal composition was calculated as a weighted mean, using the means and associated uncertainties of the different analytical techniques. The mass fraction of Sr, Y, La and Ce were calculated using a weighted mean of XRF and solution ICP-MS methods. It should be noted that where a weighted mean was used to define the P-Cal chemical composition, the individual analytical technique fully propagated uncertainties (measurement + calibration) are within 2s of each other. Elements only detectable by solution ICP-MS analysis and therefore, only defined by one analytical method are Ti, Co, Ni, Cu, Zn, Rb, Ba, Nd, Sm, Eu, Gd, Dy, Er, Yb, Lu, Pb and Th. Some variability was seen between dissolutions for solution ICP-MS of different individual chips (e.g., Y) that was outside measurement uncertainties and the averaging of seven individual chip dissolutions as well as the five powder dissolutions were done to accurately characterise the material.

The use of P-Cal for evaluation of optimal laser conditions requires a degree of compositional homogeneity that allows for investigation into LA-ICP-MS conditions without variability being dominated by sample heterogeneity. To evaluate P-Cal homogeneity, the relative standard deviation (RSD) of hundred measurements was compared with the mean analytical uncertainty ('within-run' precision output from LADR; Norris and Danyushevsky 2018) of the analytical method (Rocholl 1998, Danyushevsky *et al.* 2011, Figure 1), where a truly homogenous sample will lie on a 1 to 1 line for these two variables. This is because for homogenous materials, higher counting statistic uncertainties (due to low abundance) will lead to a correspondingly higher analysis-to-analysis variability or RSD (Figure 1). For example, the reference glass USGS BCR-2G, is relatively close to the 1:1 line for most of the measured elements and has a linear correlation consistent with the behaviour of a homogenous material. For P-Cal chips Ba, Si, Ni, Th, Pb and U are too heterogeneous or have mass fractions too close to the limit of detection of the applied methods and operational conditions in P-Cal to be useful for the purposes of this study. Figure 1b displays a series of elements in P-Cal that

have relatively good counting statistics; however, do display variable heterogeneity in the material. To overcome this slight heterogeneity for some elements (particularly Y and the HREE) hundreds of analyses were performed by LA-ICP-MS to achieve a representative sampling of P-Cal and by reducing the standard error of the mean of hundred analyses to a level consistent with or similar to the instrument mean uncertainties. Our data display a normal distribution for most elements suggesting that use of standard error in this manner is justified. A comparison of the homogeneity between the P-Cal chip and the pressed pellet analyses displays variable behaviour of elements, with some showing sufficient homogenisation (Y and HREE) while others do not (Mg, Mn, Fe, Sr, LREE). This suggests that the powder of the P-Cal chips were not fully homogenised during the grinding process and that the scale of heterogeneity is relatively large with respect to the volume sampled by the laser. The P-Cal reference values for elements shown to be sufficiently homogenous to be used in this study to evaluate the operational conditions are presented in Table 2.

### Quantification of mass fractions in calcium carbonate using different glass RMs

The choice of reference materials and calibration strategy is important to provide accurate analytical results for LA-ICP-MS (Kuhn *et al.* 2010, Nadoll and Koenig 2011, Gilbert *et al.* 2014, Redaa *et al.* 2021). To investigate the optimum reference materials and calibration strategies for LA-ICP-MS, a single set of P-Cal analyses were computed using four methodologies (A-D; Table 1). The results were then compared with the independently accepted P-Cal composition determined from XRF, EPMA and solution ICP-MS (Figure 2a). The elements deemed inhomogeneous were not included in this comparison.

Calibration methods B-D produce analytical results outside of the method uncertainties for light rare earth elements (LREE), Co and Fe (excluding calibration C, Figure 2a). Calibration method D, which includes a secondary reference material correction using USGS MACS-3 produced P-Cal compositions with the greatest degree of bias relative to the accepted composition. USGS MACS-3, though the best matrix-matched material to P-Cal calcite, produces inaccurate results compared with results calibrated using the NIST SRM 612 or basaltic glasses. This could be due to USGS MACS-3 heterogeneity or due to the ablation behaviour differences between crystal chips and powder samples (Jochum *et al.* 2019). However, the P-Cal pressed powder pellet did not display differences when compared with crystal chip analyses and this suggests the original MACS-3 is heterogeneous in composition for many elements

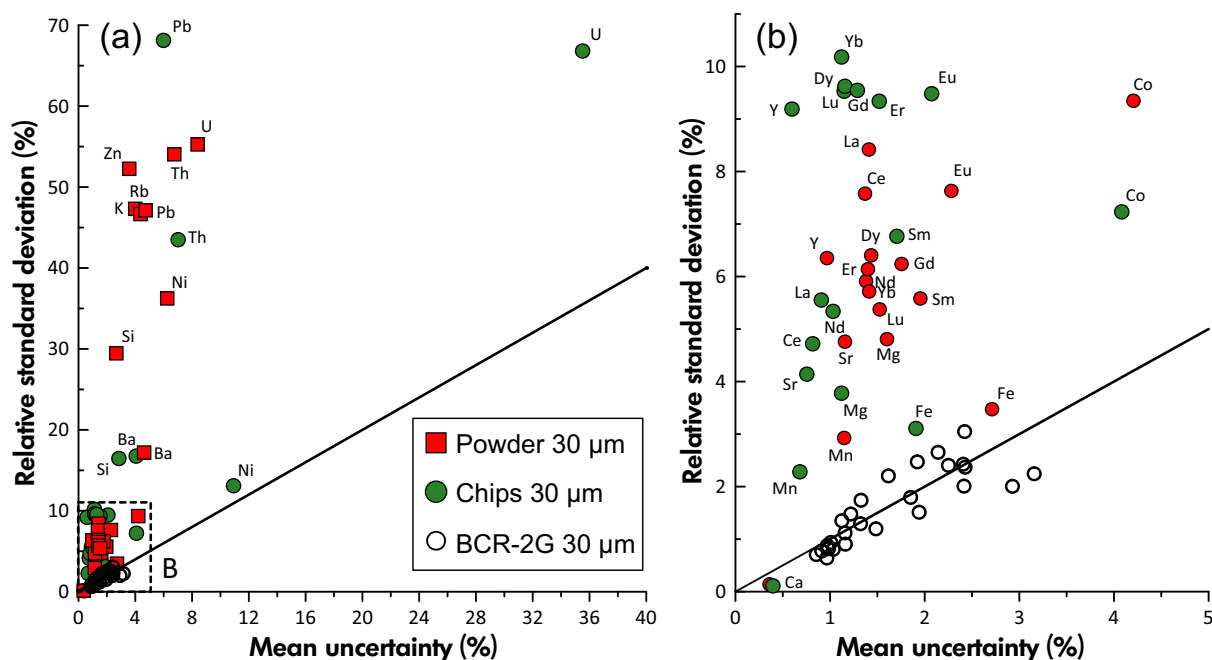


**Figure 1.** Plots assessing the homogeneity of the P-Cal sample analysed as chips at various spot sizes and as a homogenised pressed powder pellet. P-Cal chips, P-Cal pressed pellet and USGS BCR-2G analysed by LA-ICP-MS at a spot size of 30  $\mu\text{m}$ . The relative standard deviation (%) is 1 s of 100 P-Cal measurements. The mean uncertainty (%) is the 1 s 'within-run' precision exported from LADR. The within-run precision (Norris and Danyushevsky 2018) includes counting statistic uncertainty from the signal, calibration RM uncertainty and uncertainty associated with calibration misfit. (a) All data analysed. (b) A zoomed in detail of the cluster of elements with a lower relative standard deviation. The entire Plot on the right represents the box with a dashed outline of the plot on the left. USGS BCR-2G spots at 30  $\mu\text{m}$  are plotted as a reference for a relatively homogeneous material.

which is in agreement with the findings of Jochum *et al.* 2019. They have demonstrated that the RSD of repeated analyses as a measure for heterogeneity depending on the mass fractions of the investigated elements for the original USGS MACS-3 pellet were significantly higher than those determined for the MACS-3-NP. Calibration method B that uses a mean of USGS BCR-2G and USGS GSD-1G secondary reference material correction is the most accurate for Mg and many REEs, whereas a NIST SRM 612 calibration (C) produces more accurate Fe values compared with the accepted P-Cal values. Calibration method A produced P-Cal compositions indistinguishable from calibration method C and is therefore not shown in Figure 2.

There is a systematic decrease in agreement between solution ICP-MS in all LA-ICP-MS calibration methods from heavy to light REE. This trend has been observed before by Tanaka *et al.* (2007) and was interpreted to be the result of REE-rich micro-inclusions in calcite that were homogenised in solution ICP-MS analyses but not sampled by LA-ICP-MS. Another possible explanation for this behaviour of the light REE is if there were a difference in element fractionation

between light and heavy REE during LA-ICP-MS analysis; however, this behaviour has not been previously observed in LA-ICP-MS.

To assess the presence of REE-rich inclusions and their potential influence on LA-ICP-MS results, a bright phase search in BSE was conducted. This BSE search identified two REE-bearing phases, bastnaesite and monazite, that were on average 0.77 and 0.61  $\mu\text{m}^2$  in size respectively (Appendix S6). There is significant heterogeneity in the distribution of these REE phases between grains and it is possible that the bright phase search performed did not obtain a representative sampling. The sum of the area containing REE phases was compared with the total area of calcite that was searched by SEM. The proportion of surface area of bastnaesite and monazite to calcite host was 2 to 4  $\times 10^{-6}$  (Appendix S6). A mass balance calculation presented in Appendix S6 shows that the amount of REE phases identified cannot account for the observed discrepancy between La in the bulk digestion methods (XRF and solution ICP-MS) and the LA-ICP-MS results. A total of  $\sim 0.75 \mu\text{g g}^{-1}$  is estimated to be added La from the

**Table 2.**

P-Cal results of three bulk chemical methods (XRF, EPMA and solution ICP-MS), the assigned composition of P-Cal resulting from these methods, and a mean of P-Cal LA-ICP-MS results using calibration B described in the text and in Table 1

Element	Solution ICP-MS	EPMA	XRF	Calcite composition	LA-ICP-MS
Ca	384431 ± 439	387489 ± 713	385806 ± 903	385007 ± 1263	386155 ± 627
Mg	5919 ± 148	5784 ± 390	5890 ± 32	5890 ± 31	5709 ± 287
Fe	6519 ± 207	6054 ± 421	6318 ± 62	6328 ± 59	5879 ± 269
Mn	700 ± 16	673 ± 71	678 ± 6	680 ± 21	665 ± 17
Co	0.97 ± 0.05			0.97 ± 0.05	0.88 ± 0.09
Sr	138 ± 2		157 ± 5	140 ± 65	141 ± 7
Y	141 ± 10		160 ± 8	152 ± 9	144 ± 12
La	114 ± 2		129 ± 6	115 ± 4	104 ± 7
Ce	207 ± 4		213 ± 11	208 ± 7	190 ± 11
Nd	74.4 ± 2.6			74.4 ± 2.6	70.4 ± 4.0
Sm	13.4 ± 0.7			13.4 ± 0.7	12.8 ± 0.9
Eu	2.10 ± 0.16			2.10 ± 0.16	2.08 ± 0.19
Gd	14.4 ± 1.2			14.4 ± 1.2	14.7 ± 1.3
Dy	16.6 ± 1.4			16.6 ± 1.4	16.8 ± 1.5
Er	12.4 ± 1.1			12.4 ± 1.1	12.6 ± 1.2
Yb	15.6 ± 1.3			15.6 ± 1.3	15.8 ± 1.4
Lu	2.70 ± 0.21			2.70 ± 0.21	2.74 ± 0.24

presence of these minor inclusions while the discrepancy between solution ICP-MS and LA-ICP-MS is  $\sim 18 \mu\text{g g}^{-1}$ . The minor effect of these inclusions to the bulk chemistry is accounted for by the relatively high ( $\sim 100 \mu\text{g g}^{-1}$ ) mass fraction of La in calcite and the small size (sub  $\mu\text{m}$ ) of the REE-rich inclusions. The bright phase search would have had to find  $\sim 24\times$  more REE inclusions to account for the difference between La by solution ICP-MS and LA-ICP-MS.

Despite the presence of low atomic number ('light') REE phases in the calcite, their size and abundance are too small to meaningfully impact the REE-bearing calcite. Any additional REE due to the presence of bastnaesite and monazite also assumes that these phases were fully digested in the solution ICP-MS preparation methodology (3 mol  $\text{l}^{-1}$   $\text{HNO}_3$ ). It is unlikely that monazite would dissolve under the digestion conditions used for solution ICP-MS (Goncalves *et al.* 2016), so estimates of low atomic number REE phases contributions are likely to be too high if monazite was not fully digested. It is more likely that differences in elemental fractionation are the cause of the behaviour of the REE during LA-ICP-MS analysis.

Previously, studies utilising LA-ICP-MS would often measure the calibration reference material and unknowns at the same laser conditions, particularly laser spot size (Fryer *et al.* 1995, Luvizotto *et al.* 2009, Mikova *et al.* 2009, Nadoll and Koenig 2011, Jochum *et al.* 2014). Since elemental fractionation in LA-ICP-MS will change as the aspect ratio of a laser crater varies (Mank and Mason 1999), use of different sized laser spots between reference materials and

unknowns could result in inaccurate results. However, with the use of small spot sizes ( $< 30 \mu\text{m}$  diameter), the uncertainties in the calibration materials can become large due to poor counting statistics (Nadoll and Koenig 2011), increased element fractionation and increased signal drop-off; which will lead to large uncertainties in characterising instrument drift. Use of a larger ( $> 60 \mu\text{m}$ ) spot on the calibration material is ideal to minimise these issues; however, this will introduce bias in the results if smaller spot sizes are used for the unknowns. This study utilises a correction based on analyses of secondary reference materials analysed at the same conditions as the unknowns, primarily for correcting for the difference in spot size if any, but also the secondary reference materials are ideally better matrix-matched to the unknowns.

The effects of using a large versus small spot size for the primary calibration can be investigated by comparing calibration methodologies A and C. In calibration method A, the primary calibration reference material was analysed at the same spot size as the unknown (30  $\mu\text{m}$ ). In calibration method C, the calibration reference material was analysed at 60  $\mu\text{m}$  with a secondary reference material, in this case also NIST SRM 612, analysed at the same spot size of the unknown (30  $\mu\text{m}$ ). Figure 3 shows the difference in the calibration uncertainties, calculated in LADR, between these two methodologies with calibration method A showing significantly higher calibration uncertainties that would contribute to a higher total uncertainty of the analysis. This issue would be exacerbated by use of even smaller spot sizes. The calibration reference material run at a larger spot

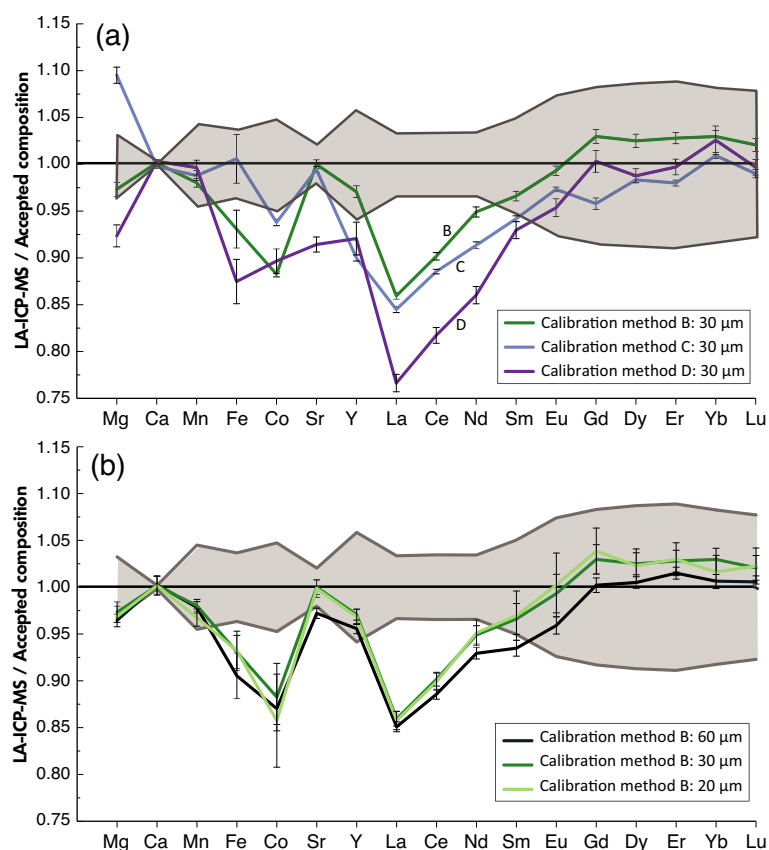


**Figure 2. (a) LA-ICP-MS P-Cal results of 100 spots at 30 µm calibrated using calibration methods B, C and D described in text. Uncertainties in this plot are one standard deviation and only include the within-run uncertainty (Norris and Danyushevsky 2018). (b) P-Cal results using three spot sizes (20, 30 and 60 µm) for one calibration method (method B was chosen). Uncertainty on individual points are within-run uncertainty. Solid line at a constant value of one defines a perfect fit between the LA-ICP-MS results and the P-Cal composition independently defined by solution ICP and XRF results. The grey shaded region is defined by the uncertainty in the P-Cal composition.**

size produces higher signal intensities and decreased signal drop-off and element fractionation, allowing for a better characterisation of any ICP-MS drift. Corrections performed using the results on secondary reference materials measured at a smaller spot size will naturally have worse counting statistics, and the uncertainties from this correction are propagated into the calibration uncertainty as shown in Figure 3. Despite this additional source of uncertainty, the total uncertainties are still lower for calibration method C compared with A. The differences in calibration method uncertainty are largely due to the ability of the primary reference material to adequately define instrument drift throughout the run.

### Optimum laser sampling conditions for accurate element analysis in carbonate

Differences in the ablation properties between different materials can lead to variable amounts of element

fractionation and therefore inaccurate results (Kuhn and Günther 2004, Marillo-Sialer *et al.* 2014). Additionally, the ablation behaviours of minerals, glasses and pressed powders can change relative to one another when varying spot size and laser fluence. The following discussion addresses the laser spot size and fluence conditions that provide the best element yield (counts per second per µg g<sup>-1</sup> element in a material) for carbonate while minimising element yield differences between the calibration materials and unknowns. The LA-ICP-MS conditions for calcium carbonate analysis presented in this study would apply to excimer 193 nm laser systems, but provides a workflow to develop similar optimal conditions for other laser systems.

As shown by Russo *et al.* (2000) increasing ablation depths can reduce the effective laser energy delivered to the sample due to (laser) plasma shielding; a contributor to element fractionation (Mao *et al.* 1996, Russo *et al.* 2002). Because of this suggested link between laser crater depths

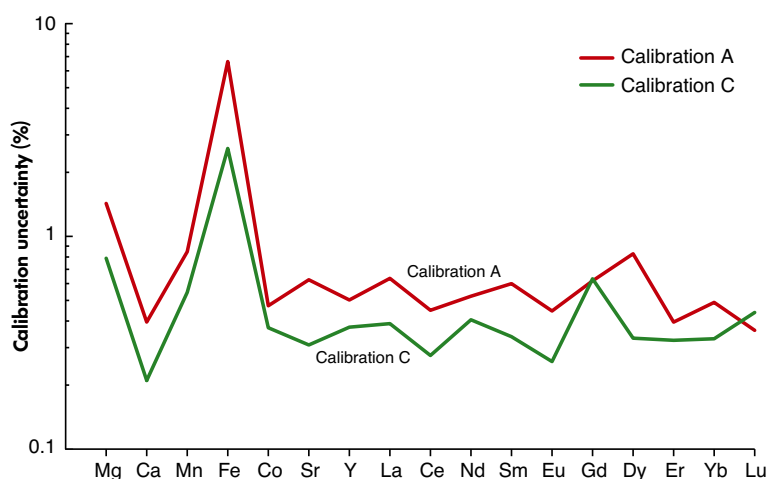


**Figure 3. Effect of calibration uncertainty when primary reference material spot size varies. The calibration uncertainty is defined by the signal uncertainty (counting statistics), on the isotope /  $^{43}\text{Ca}$  ratio for primary calibration, primary calibration drift curve misfit and variance in the secondary reference material correction factors – if applicable. Calibration A: NIST SRM 612 measured at the same spot size (30  $\mu\text{m}$ ) as P-Cal. Calibration C: NIST SRM 612 measured at a 60  $\mu\text{m}$  spot size for primary calibration and a secondary correction using the NIST SRM 612 measured at a 30  $\mu\text{m}$  spot size to correct for spot size effects. The larger spot sizes provide a more robust and lower uncertainty calibration and characterisation of instrument drift.**

and element fractionation, our study investigated the laser crater depths for USGS BCR-2G, NIST SRM 612 and the P-Cal calcite to assess changes in ablation rates between the different materials. At both large and small spot sizes, 20 and 60  $\mu\text{m}$  respectively, the laser crater depth of P-Cal is similar to NIST SRM 612 at low laser fluence and starts to diverge at laser fluence values above  $\sim 3 \text{ J cm}^{-2}$  (Figure 4a, b). Variations of spot size changed the laser ablation rate for a given material, but did not change the relationship between NIST SRM 612 and P-Cal. Figure 4c shows mean depths for three samples analysed at  $3.5 \text{ J cm}^{-2}$  laser fluence for spot sizes of 20, 30, 40 and 60  $\mu\text{m}$ , all three materials showing a decrease in ablation depth (i.e. ablation rate) with increasing spot size. USGS GSD-1G has a systematically lower ablation rate for the same laser conditions than P-Cal or NIST SRM 612. USGS BCR-2G was measured as well, but not plotted as it shows identical behaviour to USGS GSD-1G. Optically NIST SRM 612 is more similar to carbonate than USGS GSD-1G; however, several elements are better quantified against basaltic glasses than NIST SRM 612 (Figure 2a). This suggests the laser ablation rate may be less important than other parameters (e.g., particle size distribution, Guillong and Günther 2002, Kros拉克ova and Günther 2007) and that the compositional differences between a reference material and unknown do not necessarily inhibit accurate LA-ICP-MS analysis. Provided a correction is applied based on

secondary reference materials, the choice of spot size does not seem to greatly affect the accuracy of carbonate analysis (Figure 2b) in contrast to previous work (Tanaka *et al.* 2007) where it was found only larger (60  $\mu\text{m}$ ) laser spots produced accurate results.

The ablation efficiency, or element yield, measured as mass cps/ $\mu\text{g g}^{-1}$ , can be used to assess the ablation process and is a function of both the laser ablation rate and the efficiency of particle transportation or digestion and element ionisation in the ICP. The element yield of P-Cal and NIST SRM 612 for Mg, Ca, Mn and Fe (Figure 5) are relatively linear with increasing fluence, whereas the same element's yield for USGS GSD-1G behave non-linearly, with less increase in yield after about  $3.5 \text{ J cm}^{-2}$ . Most elements of interest show similar trends in changing yield with increasing laser fluence; however, for simplicity only Mg, Ca, Mn and Fe have been shown in Figure 5 as these elements are the most homogeneous in the P-Cal sample and span a range of element volatilities; previously linked to element fractionation in LA-ICP-MS (Hirata 1997, Gilbert *et al.* 2014). Based on the observations in Figure 5, the ideal fluence for the laser ablation system used in this study would be  $3.5 \text{ J cm}^{-2}$ . Higher laser fluence would cause the ablation behaviour between carbonate and reference material to diverge and lower fluence would dramatically decrease the volume of ablated material, and therefore increase the limits of

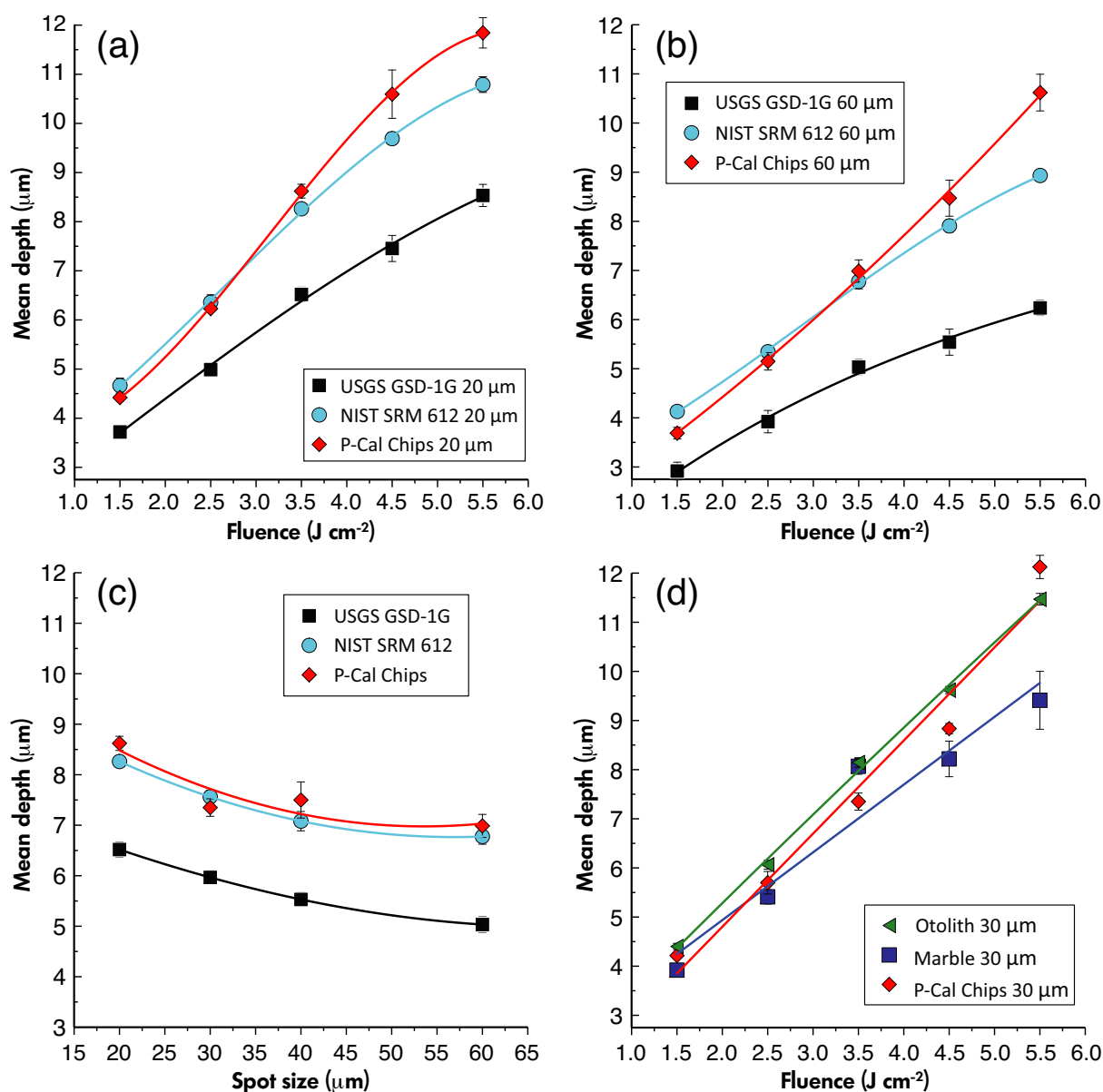


**Figure 4. Ablation depths for 20, 30 and 60 μm spot sizes, laser fluences and materials, each with 50 laser shots. (a) and (b) the relationship between laser fluence and material at 20 and 60 μm respectively. (c) Effect of changing spot size on the ablation depth for the same fluence. (d) Several calcium carbonate samples measured at various laser fluences at 30 μm. Uncertainties on the depth measurements are the standard deviation of a mean value of three laser craters.**

detection and analytical uncertainty for trace elements in carbonate. Also, lower fluence would potentially not couple as well to transparent, pure calcite (Jeffries *et al.* 1995), resulting in more mineral fracturing or lack of full ablation.

The yield and ablation rates of P-Cal closely resemble those of NIST SRM 612 but not those of USGS GSD-1G. However, an investigation into the existence of any element fractionation is necessary to better understand why most

elements are better calibrated on USGS BCR-2G (via secondary correction). We investigated element fractionation by looking at change in isotopes relative to <sup>43</sup>Ca as the laser drills down hole, similar to down-hole corrections for <sup>206</sup>Pb/<sup>238</sup>U for U-Pb dating in zircon (Paton *et al.* 2010). To remove counting statistic noise present on an individual analysis that can obscure any fractionation trends, several measurements were stacked to form a mean isotope to <sup>43</sup>Ca curve (Paton *et al.* 2010). Down-hole fraction curves of <sup>89</sup>Y,

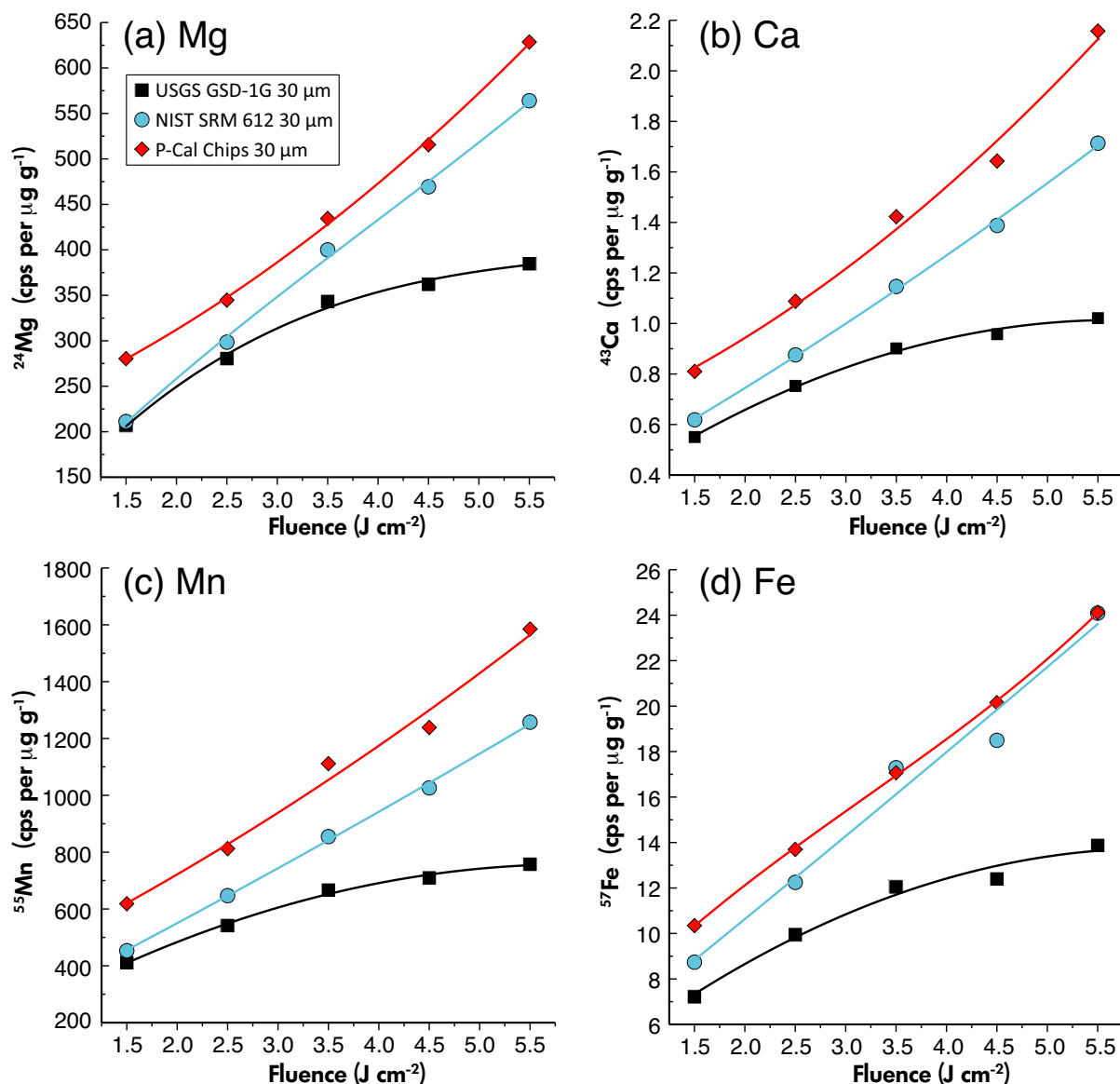


**Figure 5.** Laser ablation yield ( $\text{cps}/\mu\text{g g}^{-1}$ ) for each element for basaltic glass USGS GSD-1G, NIST SRM 612 and P-Cal calcite chips using a  $30 \mu\text{m}$  spot at various laser fluences. Figures (a) to (d) correspond to Mg, Ca, Mn and Fe respectively. The reference values for NIST SRM 612 and USGS GSD-1G are preferred values from the GeoReM database (Jochum *et al.* 2005) while the reference values for P-Cal are the compilation values presented in Table 2.

$^{140}\text{Ce}$ ,  $^{55}\text{Mn}$  and  $^{24}\text{Mg}$  are shown in Figure 6 where a ratio (isotope over  $^{43}\text{Ca}$ ) in calcite is normalised to the same ratio in reference glasses using the GeoReM preferred values (Jochum *et al.* 2005). These elements were chosen because they did not exhibit zoning in P-Cal and are in high enough mass fraction to provide robust counting statistics. Additionally, these elements span a wide range in mass, element volatility and oxide boiling point (all can influence element fractionation) and thus can be used as proxies for other elements (Fryer *et al.* 1995, Gilbert *et al.* 2017). In Figure 6, a difference in curve shape or in the positions of the curve on

the Y-axis between the different materials would suggest some variation in ablation characteristics. Both the shape and the absolute values of the down-hole fractionation curves are different between P-Cal and the reference glasses for the elements Mg, Y and Ce. Magnesium down-hole curves for NIST SRM 612 are significantly offset from P-Cal (Figure 6a) and the resulting quantification of P-Cal using NIST SRM 612 is significantly inaccurate relative to quantification against USGS BCR-2G, which has a better curve fit for Mg (Figure 6e). Cerium has the greatest down-hole trend differences between the reference glasses and P-Cal, and

quantification against either glass provides biased results outside of the method uncertainties. Manganese shows little difference in the curves between the three materials and this element shows the highest accuracy when quantified against either reference material. Changes in the shape of the curve throughout the ablation are due to element fractionation between the element of interest and Ca, the internal standard element. Correcting for time-dependent element fractionation for carbonate, as done in zircon U-Pb dating (Jackson 1996, Paton *et al.* 2010) would not appear to improve the accuracy due to systematic offsets for some elements in the curves between the different materials. These systematic offsets may be due to elemental fractionation present due to differences in particle size distribution and resulting digestion in the ICP-MS (Guilong and Günther 2002, Krosiakova and Günther 2007) for the three different matrices shown in Figure 6. However, it is also possible these systematic biases are due to large-scale heterogeneities in NIST SRM glass composition (Eggins and Shelley 2002). Future work investigating robust plasma conditions as

suggested by Fietzke and Frishe (2016) may help determine causes of systematic offsets between NIST SRM 612, USGS BCR-2G and P-Cal calcite.

As shown for quartz (Jeffries *et al.* 1995, Audétat *et al.* 2015), variable ablation properties can exist within a single mineral based upon the purity or colour variations. To examine the potential applicability of P-Cal results to other calcium carbonate samples, laser crater depths were measured on a coarse marble and a fish otolith sample (aragonite). The ablation crater depths diverge at high laser fluence with the marble sample producing shallow craters compared with the fish otolith and P-Cal (Figure 4d). This difference in ablation depths is not significant compared with the differences between calcite and reference glasses as shown in Figure 4a–c and would suggest that even at higher fluences, there would be little systematic bias in the results between different carbonate matrixes. However, use of higher fluences is not optimum for ablation of basaltic glasses used as secondary

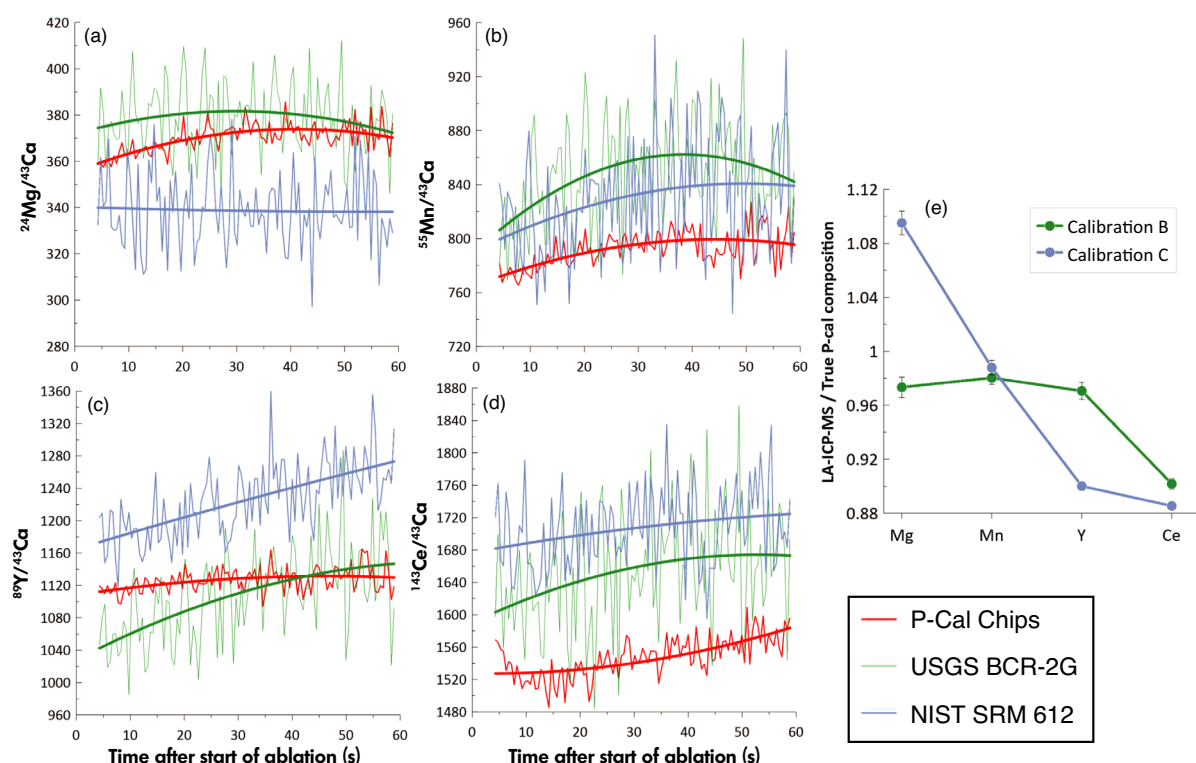


**Figure 6.** Stacked down-hole curves (a–d) using methodology of Paton *et al.* (2010) for  $^{24}\text{Mg}$ ,  $^{55}\text{Mn}$ ,  $^{89}\text{Y}$  and  $^{140}\text{Ce}$  all relative to  $^{43}\text{Ca}$  for P-Cal chip analyses ( $n = 23$ ), USGS BCR-2G ( $n = 6$ ) and NIST SRM 612 ( $n = 6$ ). Comparison of measured to the accepted values for Mn, Mn, Y, and Ce concentrations in P-Cal (e). All measurements were performed at a laser spot size of  $30\ \mu\text{m}$ . Curves are shown normalised to the isotope/Ca  $\mu\text{g g}^{-1}$  values for each material. Uncertainties are one standard deviation.

reference materials. Additionally, higher fluences will result in higher ablation rates causing increased signal drop-off due and potentially ablating a higher number of inclusions if present in a sample.

### Comparison of LA-ICP-MS measurement results for calcite pressed powder and calcite chips

P-Cal was prepared as a pressed powder and whole mineral chips (a few mm in diameter) that were both analysed by LA-ICP-MS to assess any impact in changing the physical matrix of the sample (powder versus crystalline material). The results for powder versus chip P-Cal are presented in Figure 7 along with USGS MACS-3, a carbonate reference material made available as a pressed pellet. Both pressed powder samples in Figure 7 have a higher ablation rate, significantly higher than P-Cal chips. However, no systematic difference in accuracy is seen between P-Cal chips and powder, despite the significant differences in ablation rate (Figure 7b). This indicates that ablation rate is of lesser importance in controlling element fractionation for the mineral calcite, contrasting with U-Pb dating of zircon where there is a significant impact on the

ablation rate and the degree of U-Pb fractionation (Marillo-Sialer *et al.* 2014).

Calibration method D, where USGS MACS-3 is the primary calibration material, produced more inaccurate results compared with those using glass reference materials (Figure 2a). Quantification of P-Cal against USGS MACS-3 produced systematically biased lower mass fractions for most elements (except Mn and HREE). Using NIST SRM 612 to calibrate USGS MACS-3 produces measured results ~ 10% different from the preferred values of GeoReM (results in Appendix S5). This offset in MACS-3 seen in this study is broadly consistent with previous studies analysing MACS-3 using silicate reference materials (Chen *et al.* 2011, Jochum *et al.* 2012). For example, our MACS-3 results show similar offsets in Mg and La to Jochum *et al.* 2012. However, our results for Fe and Sr are significantly different from Jochum *et al.* 2012 and given the similarity in element properties of Sr and Ca, we suggest this is likely due to heterogeneities in MACS-3 in different laboratories. The decrease in accuracy shown in Figure 2a when P-Cal is calibrated to USGS MACS-3 suggests that USGS MACS-3 material is poorly suited for calibration purposes compared with the reference

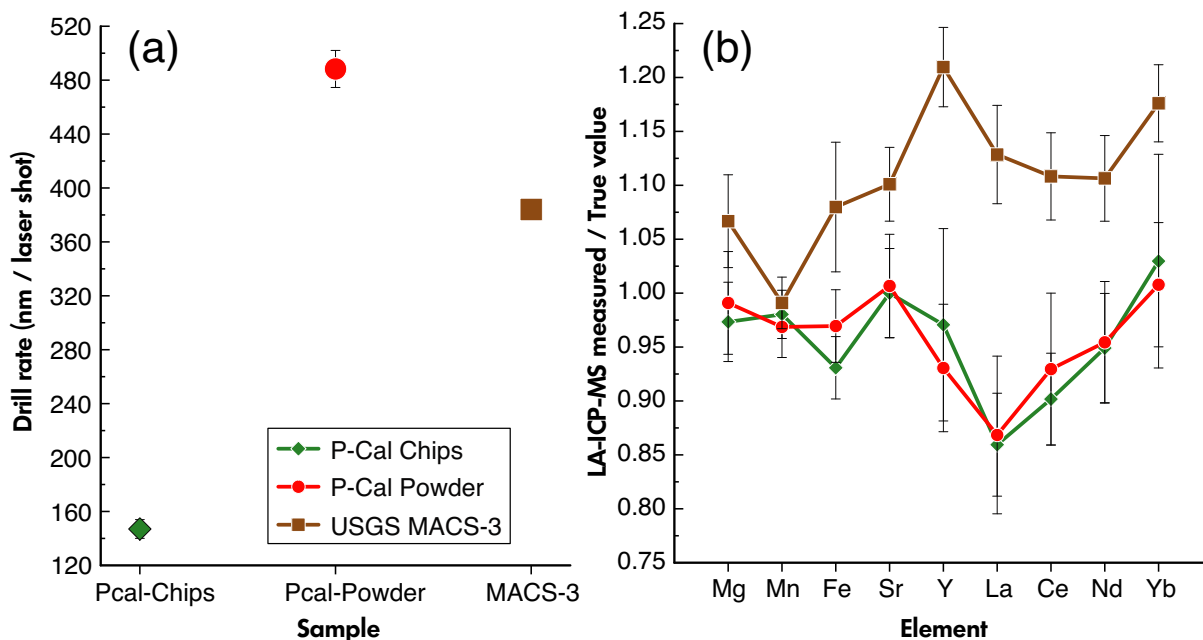


**Figure 7. (a) Ablation rate measurements for P-Cal chips, P-Cal powder and USGS MACS-3. Sample standard deviation and mean of three analyses. (b) Selected elements in P-Cal measured by LA-ICP-MS as chips and as a pressed powder pellet normalised to the expected value for a 30 µm spot calibrated using NIST SRM 612 at a 60 µm spot size and secondary reference material corrected using USGS BCR-2G and USGS GSD-1 G. Also plotted is USGS MACS-3 treated as an unknown. Uncertainties are the relative standard deviation of the mean (100 analyses for P-Cal chips and pressed powder, fifteen analyses on USGS MACS-3).**

glasses used in this study (Figure 7b). This is likely due to heterogeneity in the MACS-3 material, leading to production of nanoparticle sized MACS-3 (Jochum *et al.* 2019) to aide in homogenisation. The results here suggest there may also be pellet-to-pellet heterogeneity in MACS-3.

The results for pressed powders show a different ablation behaviour to unaltered crystal chips (Figure 7) with a significantly higher ablation rate in the former. However, the yield remains identical between the pressed powder and the chips (Appendix S4). This suggests that the excess particles removed during ablation of the pressed powders are not transported to the ICP due to their larger size. If the particles were transported to the ICP and not fully digested, there likely would have been a compositional difference between pressed powder and mm sized chip; correlating with element volatility or oxide boiling point.

### Correction factors

Despite most elements resulting in an accurate analysis using calibration method B, there are some systematic biases outside the assigned uncertainties of the P-Cal accepted values and the uncertainties from the LA-ICP-MS measurements for elements Fe, Co, La, Ce, Nd (Figure 2). Past studies such as Tanaka *et al.* (2007) and Chen *et al.* (2011) have considered LA-ICP-MS suitable and the results accurate if the measured data agree within  $\pm 10\%$  with published or reference values, defined by a quality control material such as USGS MACS-3 regardless of the measurement precision. However, in an effort to make the LA-ICP-MS technique more quantitative, this study has assessed measurement bias based on the fully propagated uncertainties between the LA-ICP-MS measurements and the accepted material composition (Gilbert *et al.* 2013). Correction factors are recommended, similar to Danyushevsky *et al.* (2011), for the elements systematically offset outside of uncertainty. Correction factors have been estimated from several LA-ICP-MS sessions using calibration method B and the laser conditions listed above. These correction factors in our study were as follows:  $0.92 \pm 0.03$  (Fe),  $0.88 \pm 0.02$  (Co),  $0.85 \pm 0.02$  (La),  $0.90 \pm 0.02$  (Ce) and  $0.95 \pm 0.02$  (Nd). The presence of light REE phases is assumed to have a negligible impact on these correction factors based on their quantitative abundance measurements by bright phase BSE search described above. These factors and uncertainties can be input directly to the data reduction software LADR to provide a fully quantitative analysis for carbonate. However, these factors would only apply to carbonate analysed with the analytical conditions suggested above and the LA-ICP-MS instrumentation used. These values would be constant for the same instrumentation and analytical conditions but should be re-assessed when these variables

change. P-Cal is not recommended as a calibration reference material, but it is useful in identifying the optimal laser conditions for calcium carbonate minerals and as a quality control material when sufficient analyses are performed.

### Conclusions

The composition of an in-house calcite sample has been determined by multiple methods, including solution ICP-MS, XRF and EPMA. This sample was then used to assess various calibration methods, spot size and laser energy parameters to define the optimal conditions in our laboratory for the analysis of calcium carbonate by LA-ICP-MS using the specified instrumentation. For many elements, primary calibration using NIST SRM 612 and a secondary calibration using reference materials USGS GSD-1G and USGS BCR-2G (calibration B) provides the best accuracy for P-Cal analysis. The ablation rate and yield of calcite was found to be similar to NIST SRM 612, but the down-hole fractionation curves for element ratio to  $^{43}\text{Ca}$  of calcite have absolute values similar to basaltic glasses (e.g., USGS GSD-1G); suggesting the ablation rate differences between calcite and glass are of lesser importance in controlling element fractionation differences between these materials. We suggest that with this instrumentation, a laser energy fluence of  $3.5 \text{ J cm}^{-2}$  should be used to analyse basaltic glass reference materials and carbonate minerals. The methodology presented here provides accurate analysis of carbonate by LA-ICP-MS for a wide range of spot sizes (60–20  $\mu\text{m}$ ) provided additional reference materials are measured at same laser conditions as unknowns for a secondary calibration. Using the calibration and analytical methodology described here, we have derived correction factors for several elements in calcite to provide a fully accurate and quantitative analysis by LA-ICP-MS applicable to the described settings and instrumentation. There is no systematic offset for P-Cal powder compared with P-Cal chips, suggesting the use of powdered materials of carbonates is justified for accurate analysis. However, the use of USGS MACS-3 as a calibration material was shown to produce systematic biases in the P-Cal results and this suggests glass reference materials are better suited for calibration of LA-ICP-MS carbonate analyses, despite the closer matrix match of USGS MACS-3 to carbonate samples. P-Cal is not suggested as a calibration material, but is available upon request from CODES Analytical Laboratories to define correction factors and optimal analytical conditions in other laboratories.

### Acknowledgements

We would like to thank Ivan Belousov at the CODES analytical laboratories for his assistance with LA-ICP-MS analyses. This manuscript was vastly improved by

reviews by Regina Mertz-Kraus and two anonymous reviewers.

## Data availability statement

The data that support the findings of this study are available in the supplementary material of this article.

## References

- Audétat A., Garbe-Schönberg D., Kronz A., Petke T., Rusk B., Donovan J.J. and Lowers H.A. (2015)**  
Characterisation of a natural quartz crystal as a reference material for microanalytical determination of Ti, Al, Li, Fe, Mn, Ga and Ge. *Geostandards and Geoanalytical Research*, **39**, 171–184.
- Barker S.L.L. and Cox S.F. (2011)**  
Oscillatory zoning and trace element incorporation in hydrothermal minerals: Insights from calcite growth experiments. *Geofluids*, **11**, 48–56.
- Barnet J.S.K., Harper D.T., LeVay L.J., Edgar K.M., Henehan M.J., Babila T.L., Ullmann C.V., Leng M.J., Kroon D., Zachos J.C. and Littler K. (2020)**  
Coupled evolution of temperature and carbonate chemistry during the Paleocene–Eocene: New trace element records from the low latitude Indian Ocean. *Earth and Planetary Science Letters*, **545**, 116414.
- Browne B.L., Eichelberger J.C., Patino L.C., Vogel T.A., Uto K. and Hoshizumi H. (2006)**  
Magma mingling as indicated by texture and Sr/Ba ratios of plagioclase phenocrysts from Unzen volcano, SW Japan. *Journal of Volcanology and Geothermal Research*, **154**, 103–116.
- Chen L., Liu Y., Hu Z., Gao S., Zong K. and Chen H. (2011)**  
Accurate determinations of fifty-four major and trace elements in carbonate by LA-ICP-MS using normalization strategy of bulk components as 100%. *Chemical Geology*, **284**, 283–295.
- Danyushevsky L., Robinson P., Gilbert S., Norman M., Large R., McGoldrick P. and Shelley M. (2011)**  
Routine quantitative multi-element analysis of sulphide minerals by laser ablation ICP-MS: Standard development and consideration of matrix effects. *Geochemistry: Exploration, Environment, Analysis*, **11**, 51–60.
- Druffel E.R.M. (1997)**  
Geochemistry of corals: Proxies of past ocean chemistry, ocean circulation and climate. *Proceedings of the National Academy of Sciences*, **94**, 8354.
- Eggins S.M. and Shelley J.M.G. (2002)**  
Compositional heterogeneity in NIST SRM 610–617 glasses. *Geostandards Newsletter: The Journal of Geostandards and Geoanalysis*, **26**, 269–286.
- Falloon T.J., Danyushevsky L.V., Crawford T.J., Maas R., Woodhead J.D., Eggins S.M., Bloomer S.H., Wright D.J., Zlobin S.K. and Stacey A.R. (2007)**  
Multiple mantle plume components involved in the petrogenesis of subduction-related lavas from the northern termination of the Tonga Arc and northern Lau Basin: Evidence from the geochemistry of arc and backarc submarine volcanics. *Geochemistry Geophysics Geosystems*, **8**, Q09003.
- Fietzke J. and Frische M. (2016)**  
Experimental evaluation of elemental behavior during LA-ICP-MS: Influences of plasma conditions and limits of plasma robustness. *Journal of Analytical Atomic Spectrometry*, **31**, 234–244.
- Frimmel H.E. (2009)**  
Trace element distribution in Neoproterozoic carbonates as palaeoenvironmental indicator. *Chemical Geology*, **258**, 338–353.
- Fryer B.J., Jackson S.E. and Longerich H.P. (1993)**  
The application of laser ablation microprobe-inductively coupled plasma-mass spectrometry (LAM-ICP-MS) to *in situ* (U)-Pb geochronology. *Chemical Geology*, **109**, 1–8.
- Fryer B.J., Jackson S.E. and Longerich H.P. (1995)**  
The design, operation and role of the laser-ablation microprobe coupled with an inductively coupled plasma-mass spectrometer (LAM-ICP-MS) in the Earth sciences. *The Canadian Mineralogist*, **33**, 303–312.
- Gaboardi M., Humayun M. (2009)**  
Elemental fractionation during LA-ICP-MS analysis of silicate glasses: Implications for matrix-independent standardization. *Journal of Analytical Atomic Spectrometry*, **24**, 1188.
- Gilbert S.E., Danyushevsky L.V., Goemann K. and Death D. (2014)**  
Fractionation of sulphur relative to iron during laser ablation-ICP-MS analyses of sulphide minerals: Implications for quantification. *Journal of Analytical Atomic Spectrometry*, **29**, 1024–1033.
- Gilbert S., Danyushevsky L., Robinson P., Wohlgemuth-Ueberwasser C., Pearson N., Savard D., Norman M. and Hanley J. (2013)**  
A comparative study of five reference materials and the Lombard meteorite for the determination of the platinum-group elements and gold by LA-ICP-MS. *Geostandards and Geoanalytical Research*, **37**, 51–64.
- Gilbert S., Olin P., Thompson J., Lounejeva E. and Danyushevsky L. (2017)**  
Matrix dependency for oxide production rates by LA-ICP-MS. *Journal of Analytical Atomic Spectrometry*, **32**, 638–646.
- Gonçalves G.O., Lana C., Scholz R., Buick I.S., Gerdes A., Kamo S.L., Corfu F., Marinho M.M., Chaves A.O., Valeriano C. and Nalini H.A. Jr (2016)**  
An assessment of monazite from the Itambé pegmatite district for use as U-Pb isotope reference material for microanalysis and implications for the origin of the “Moacyr” monazite. *Chemical Geology*, **424**, 30–50.
- Griffiths M.L., Drysdale R.N., Gagan M.K., Frisia S., Zhao J.-X., Ayliffe L.K., Hantoro W.S., Hellstrom J.C., Fischer M.J., Feng Y.-X. and Suwargadi B.W. (2010)**  
Evidence for Holocene changes in Australian-Indonesian monsoon rainfall from stalagmite trace element and stable isotope ratios. *Earth and Planetary Science Letters*, **292**, 27–38.

## references

---

- Guillong M. and Günther D. (2002)**  
Effect of particle size distribution on ICP-induced elemental fractionation in laser ablation-inductively coupled plasma-mass spectrometry. *Journal of Analytical Atomic Spectrometry*, 17, 831–837.
- Hathorne E.C., James R.H., Savage P. and Alard O. (2008)**  
Physical and chemical characteristics of particles produced by laser ablation of biogenic calcium carbonate. *Journal of Analytical Atomic Spectrometry*, 23, 240–243.
- He D., Lee C.-T.-A., Yu X. and Famer M. (2019)**  
Ge/Si partitioning in igneous systems: Constraints from laser ablation ICP-MS measurements on natural samples. *Geochemistry Geophysics Geosystems*, 20, 4472–4486.
- Hirata T. (1997)**  
Ablation technique for laser ablation-inductively coupled plasma-mass spectrometry. *Journal of Analytical Atomic Spectrometry*, 12, 1337–1342.
- Izbekov P.E., Eichelberger J.C., Patino L.C., Vogel T.A. and Ivanov B.V. (2002)**  
Calcic cores of plagioclase phenocrysts in andesite from Karymsky volcano: Evidence for rapid introduction by basaltic replenishment. *Geology*, 30, 799–802.
- Jackson S.E. (1996)**  
The application of laser ablation microprobe (LAM)-ICP-MS to *in situ* U-Pb zircon geochronology. *Journal of Conference Abstracts*, 1, 283.
- Jackson S.E., Pearson N.J., Griffin W.L. and Belousova E.A. (2004)**  
The application of laser ablation-inductively coupled plasma-mass spectrometry to *in situ* U-Pb zircon geochronology. *Chemical Geology*, 211, 47–69.
- Jarosewich E. and Macintyre I.G. (1983)**  
Carbonate reference samples for electron microprobe and scanning electron microscope analyses. *Journal of Sedimentary Research*, 53, 677–678.
- Jeffries T.E., Perkins W.T. and Pearce N.J.G. (1995)**  
Comparisons of infrared and ultraviolet laser probe microanalysis inductively coupled plasma-mass spectrometry in mineral analysis. *Analyst*, 120, 1365–1371.
- Jochum K.P., Game-Schönberg D., Vetter M., Stoll B., Weis U., Weber M., Lugli F., Jentzen A., Schiebel R., Wassenburg J.A., Jacob D.E. and Haug G.H. (2019)**  
Nano-powdered calcium carbonate reference materials: Significant progress for microanalysis. *Geostandards and Geoanalytical Research*, 43, 595–609.
- Jochum K.P., Nohl U., Herwig K., Lammel E., Stoll B. and Hofmann A.W. (2005)**  
GeoReM: A new geochemical database for reference materials and isotopic standards. *Geostandards and Geoanalytical Research*, 29, 333–338.
- Jochum K.P., Scholz D., Stoll B., Weis U., Wilson S.A., Yang Q., Schwalb A., Bömer N., Jacob D.E. and Andreae M.O. (2012)**  
Accurate trace element analysis of speleothems and biogenic calcium carbonates by LA-ICP-MS. *Chemical Geology*, 318–319, 31–44.
- Jochum K.P., Stoll B., Weis U., Jacob D.E., Mertz-Kraus R. and Andreae M.O. (2014)**  
Non-matrix-matched calibration for the multi-element analysis of geological and environmental samples using 200 nm Femtosecond LA-ICP-MS: A comparison with nanosecond lasers. *Geostandards and Geoanalytical Research*, 38, 265–292.
- Jochum K.P., Weis U., Stoll B., Kuzmin D., Yang Q., Raczek I., Jacob D.E., Stracke A., Birbaum K., Frick D.A., Günther D. and Enzweiler J. (2011)**  
Determination of reference values for NIST SRM 610–617 glasses following ISO guidelines. *Geostandards and Geoanalytical Research*, 35, 397–429.
- Kalliomäki H., Wagner T., Fusswinkel T. and Schultze D. (2019)**  
Textural evolution and trace element chemistry of hydrothermal calcites from Archean gold deposits in the Hattu schist belt, eastern Finland: Indicators of the ore-forming environment. *Ore Geology Reviews*, 112, 103006.
- Kontak D. and Jackson S. (1995)**  
Laser-ablation ICP-MS micro-analysis of calcite cement from a Mississippi-Valley-Type Zn-Pb deposit, Nova Scotia: Dramatic variability in REE content on macro and micro scales. *The Canadian Mineralogist*, 33, 445–467.
- Košler J., Jackson S.E., Yang Z. and Wirth R. (2014)**  
Effect of oxygen in sample carrier gas on laser-induced elemental fractionation in U-Th-Pb zircon dating by laser ablation ICP-MS. *Journal of Analytical Atomic Spectrometry*, 29, 832–840.
- Kroslakova I. and Günther D. (2007)**  
Elemental fractionation in laser ablation-inductively coupled plasma-mass spectrometry: Evidence for mass load induced matrix effects in the ICP during ablation of a silicate glass. *Journal of Analytical Atomic Spectrometry*, 22, 51–62.
- Kuhn B.K., Birbaum K., Luo Y. and Günther D. (2010)**  
Fundamental studies on the ablation behaviour of Pb/U in NIST 610 and zircon 91500 using laser ablation inductively coupled plasma-mass spectrometry with respect to geochronology. *Journal of Analytical Atomic Spectrometry*, 25, 21–27.
- Kuhn H.R. and Günther D. (2004)**  
Laser ablation-ICP-MS: Particle size dependent elemental composition studies on filter-collected and online measured aerosols from glass. *Journal of Analytical Atomic Spectrometry*, 19, 1158–1164.



## references

---

**Leslie R.A.J., Danyushevsky L.V., Crawford A.J. and Verbeeten A.C. (2009)**

Primitive shoshonites from Fiji: Geochemistry and source components. *Geochemistry Geophysics Geosystems*, 10, Q07001.

**Leys C.A., Cloos M., New B.T.E. and MacDonald G.D. (2012)**

Copper-gold +/- molybdenum deposits of the Ertzberg-Grasberg district, Papua, Indonesia. *Society of Economic Geologists Special Publication*, 16, 215–235.

**Longerich H.P., Jackson S.E. and Günther D. (1996)**

Inter-laboratory note. Laser ablation inductively coupled plasma-mass spectrometric transient signal data acquisition and analyte concentration calculation. *Journal of Analytical Atomic Spectrometry*, 11, 899–904.

**Luvizotto G.L., Zack T., Meyer H.P., Ludwig T., Triebold S., Kronz A., Münker C., Stöckli D.F., Prowatke S., Klemme S., Jacob D.E. and von Eynatten H. (2009)**

Rutile crystals as potential trace element and isotope mineral standards for microanalysis. *Chemical Geology*, 261, 346–369.

**Mank A.J.G. and Mason P.R.D. (1999)**

A critical assessment of laser ablation ICP-MS as an analytical tool for depth analysis in silica-based glass samples. *Journal of Analytical Atomic Spectrometry*, 14, 1143–1153.

**Mao X., Chan W.T., Caetano M., Shannon M.A. and Russo R.E. (1996)**

Preferential vaporization and plasma shielding during nano-second laser ablation. *Applied Surface Science*, 96–98, 126–130.

**Marillo-Sialer E., Woodhead J., Hergt J., Greig A., Guillong M., Gleadow A., Evans N. and Paton C. (2014)**

The zircon 'matrix effect': Evidence for an ablation rate control on the accuracy of U-Pb age determinations by LA-ICP-MS. *Journal of Analytical Atomic Spectrometry*, 29, 981–989.

**McGuire A.V., Francis C.A. and Dyar M.D. (1992)**

Mineral standards for electron microprobe analysis of oxygen. *American Mineralogist*, 77, 1087–1091.

**Mertz-Kraus R., Brachert T.C., Jochum K.P., Reuter M. and Stoll B. (2009)**

LA-ICP-MS analyses on coral growth increments reveal heavy winter rain in the eastern Mediterranean at 9 Ma. *Palaeogeography, Palaeoclimatology, Palaeoecology*, 273, 25–40.

**Mikova J., Košler J., Longerich H.P., Wiedenbeck M. and Hancher J.M. (2009)**

Fractionation of alkali elements during laser ablation ICP-MS analysis of silicate geological samples. *Journal of Analytical Atomic Spectrometry*, 24, 1244–1252.

**Mitsuguchi T., Matsumoto E., Abe O., Uchida T. and Isdale P.J. (1996)**

Mg/Ca thermometry in coral skeletons. *Science*, 274, 961–963.

**Müller W., Shelley M., Miller P. and Broude S. (2009)**

Initial performance metrics of a new custom-designed ArF excimer LA-ICP-MS system coupled to a two-volume laser-ablation cell. *Journal of Analytical Atomic Spectrometry*, 24, 209–214.

**Nadoll P. and Koenig A.E. (2011)**

LA-ICP-MS of magnetite: Methods and reference materials. *Journal of Analytical Atomic Spectrometry*, 26, 1872–1877.

**Norris C.A. and Danyushevsky L. (2018)**

Towards estimating the complete uncertainty budget of quantified results measured by LA-ICP-MS. *Goldschmidt Conference Abstracts (Boston, Massachusetts)*, 1894.

**Oliver N.H.S., Cartwright I., Wall V.J. and Golding S.D. (1993)**

The stable isotope signature of kilometre-scale fracture dominated metamorphic fluid pathways, Mary Kathleen, Australia. *Journal of Metamorphic Geology*, 11, 705–720.

**Page R.W. (1983)**

Chronology of magmatism, skarn formation and uranium mineralization, Mary Kathleen, Queensland, Australia. *Economic Geology*, 78, 838–853.

**Paton C., Woodhead J.D., Hellstrom J.C., Hergt J.M., Greig A. and Maas R. (2010)**

Improved laser ablation U-Pb zircon geochronology through robust downhole fractionation correction. *Geochemistry Geophysics Geosystems*, 11, Q0AA06.

**Redaa A., Farkaš J., Gilbert S., Collins A.S., Wade B., Lohr S., Zack T. and Garbe-Schönberg D. (2021)**

Assessment of elemental fractionation and matrix effects during *in situ* Rb-Sr dating of phlogopite by LA-ICP-MS/MS: Implications for the accuracy and precision of mineral ages. *Journal of Analytical Atomic Spectrometry*, 36, 322–344.

**Rocholl A. (1998)**

Major and trace element composition and homogeneity of microbeam reference material: Basalt glass USGS BCR-2G. *Geostandards Newsletter: The Journal of Geostandards and Geoanalysis*, 22, 33–45.

**Russo R.E., Mao X.L., Borisov O.V. and Liu H. (2000)**

Influence of wavelength on fractionation in laser ablation ICP-MS. *Journal of Analytical Atomic Spectrometry*, 15, 1115–1120.

**Russo R.E., Mao X.L. and Mao S.S. (2002)**

The physics of laser ablation in microchemical analysis. *Analytical Chemistry*, 74, 70–77.

**Štírad L., Etlér V., Mihaljević M., Hladil J. and Chrástný V. (2009)**

Determination of trace elements in calcite using solution and laser ablation ICP-MS: Calibration to NIST SRM glass and USGS MACS carbonate, and application to real landfill calcite. *Geostandards and Geoanalytical Research*, 33, 347–355.

## references

---

- Tanaka K., Takahashi Y. and Shimizu H. (2007)**  
Determination of rare earth element in carbonate using laser ablation inductively coupled plasma-mass spectrometry: An examination of the influence of the matrix on laser ablation-inductively coupled plasma-mass spectrometry analysis. *Analytica Chimica Acta*, **583**, 303–309.
- Thompson J.M., Houk R.S., Olin P.H., Fryer F. and Danyushevsky L.V. (2020)**  
The effects of H<sub>2</sub>O, He, N<sub>2</sub> and H<sub>2</sub> on ion kinetic energies in inductively coupled plasma-mass spectrometry. *Spectrochimica Acta Part B*, **169**, 105870.
- Tremaine D.M. and Froelich P.N. (2013)**  
Speleothem trace element signatures: A hydrologic geochemical study of modern cave dripwaters and farmed calcite. *Geochimica et Cosmochimica Acta*, **121**, 522–545.
- Vaughan J.R., Hickey K.A. and Barker S.L.L. (2016)**  
Isotopic, chemical and textural evidence for pervasive calcite dissolution and precipitation accompanying hydrothermal fluid flow in low-temperature, carbonate-hosted, gold systems. *Economic Geology*, **111**, 1127–1157.
- Wyndham T., McCulloch M., Fallon S. and Alibert C. (2004)**  
High-resolution coral records of rare earth elements in coastal seawater: Biogeochemical cycling and a new environmental proxy. *Geochimica et Cosmochimica Acta*, **68**, 2067–2080.

## Supporting information

---

The following supporting information may be found in the online version of this article:

Appendix S1. XRF measurement results for P-Cal.

Appendix S2. Solution ICP-MS measurement results for P-Cal.

Appendix S3. EPMA measurement results.

Appendix S4. Laser ablation measurement results for the different calibration methods.

Appendix S5. Measurement results for element mass fractions in MACS-3 calibrated against NIST SRM 612.

Appendix S6. Bright phase search by BSE mapping and subsequent EDS analysis.

This material is available from: <http://onlinelibrary.wiley.com/doi/10.1111/ggr.12405/abstract> (This link will take you to the article abstract).

